An energy-efficient scalar control taking core losses into account

Gabriel Khoury, Ragi Ghosn, Flavia Khatounian, Maurice Fadel, Mathias Tientcheu

AN ENERGY EFFICIENT SCALAR CONTROL STRUCTURE TAKING CORE LOSSES INTO ACCOUNT

Gabriel Khoury[1,2], Ragi Ghosn[1], Flavia Khatounian[1], Maurice Fadel[2], Mathias Tientcheu[3]

1. CINET, ESIB, Université Saint-Joseph de Beyrouth, 11-514, 1107 2050, Beirut, Lebanon.
e-mail: gabriel.khoury@usj.edu.lb, ragi.ghosn@usj.edu.lb, flavia.khatounian@usj.edu.lb

2. LAPLACE, Université de Toulouse, CNRS, INPT, UPS, 2 rue Charles Camichel, 31071, Toulouse, France.
e-mail: maurice.fadel@laplace.univ-tlse.fr

3. Leroy Somer, Angoulême, France.
e-mail: mathias.tientcheuyamdeu@emerson.com

Abstract – Control structures are the main actor for energy efficiency optimization of electric motors, which depends on the operating point and the mechanical load of the motor. The scope of this paper is to present an energy efficient optimized scalar control structure for the squirrel-cage induction motor (IM), taking into consideration the effect of the motor core losses. The proposed technique is based on the modification of the stator flux reference according to the operating point, in order to track the best efficiency point. The optimal values of flux are computed through an improved model of the induction motor including core losses. The proposed scalar control is simulated showing the improvement in energy efficiency, which is then validated through experimental results conducted on two induction motors of different generations and compliant with different efficiency standards.

Keywords – Induction motor, energy efficiency, optimization, power losses, scalar control.

1. INTRODUCTION

Energy efficiency optimization has become nowadays the goal of many researches, especially for electrical systems. This goal can be achievedin several ways, either by working on the improvement of the electrical elements themselve, either by action on the control. The European Climate & Energy package for instance, has set itself a 20% energy savings target by 2020, and motor standards were established to classify high efficiency IE2 and premium efficiency IE3 motors, setting a goal for all produced motors to be compliant with IE3 by 2017. These standards define the maximum reachable motor efficiency at rated speed and torque operation. The efficiency decreases at other operating points, but can yet be optimized through the control drive. Therefore, the goal of several studies is to improve the classic control drives in order to maintain the best energy efficiency in all operating conditions.

Several improvement methods relative to the energy efficiency of induction motors are discussed in literature, most of which are resumed in a review presented in [1]. Some listed techniques rely on artificial intelligence and nature inspired algorithms as new technologies used for optimization, whereas the main presented structures are the Loss Minimization Control (LMC) and the Search Control (SC), which are detailed later. These methods are proved to optimize the energy efficiency. They offer as well the advantage to be compatible with both scalar or vector controlled structures.

The search control is detailed in [2] and applied to a scalar controlled IM. Its aim is tracking the lowest possible input power of the motor by applying small modifications to the stator flux and comparing the power value to the previous state. Experimental tests show an improvement of the motor efficiency and a decrease in the motor losses.

The loss minimization control is established in [3], it estimates the power losses through specific models and computes the zeros of the total loss derivative. The corresponding optimal flux reference is then calculated and applied to the motor in order to get the best energy efficiency. Simulation results show that the LMC optimization algorithm increases the efficiency especially in the cases of reduced load torques.

In another approach, a fuzzy logic technique tracking the best efficiency is proposed in [4], where the input voltage is modified according to a defined rule, in order to track the highest efficiency operating point in given conditions. Simulation results show that the efficiency increases at low voltages while operating at low load torque.

The best efficiency point tracking can also be done through the Maximum Torque Per Ampere (MTPA) algorithm detailed in [5]. It is based on the slip angular frequency versus torque curve which is computed to verify the MTPA strategy, and applied to a scalar controlled induction motor. Losses are estimated as well as the efficiency, and experimental results show the expected efficiency increase and losses decrease. Ref. [6] presents a similar control system based on the MTPA algorithm aiming to maintain an optimal flux in the motor. Simulations results are compared to those of the classic scalar control to validate the optimized efficiency and the reduced losses.

The proposed improvement methods are proved to optimize the energy efficiency of induction motors and reduce their losses. However, the effect of core losses is generally either omitted or taken into consideration through an approximate approach. In this paper, a novel method of tracking the best efficiency point is applied to the classic scalar control. It is based on an improved dynamic model of the squirrel-cage induction motor taking into account variable core losses. The stator flux reference is therefore modified throughout the motor operation according to a look-up table, computed to give the best energy efficiency at given operating conditions.

In section 2, the induction motor dynamic model including variable core losses is presented, as well as the optimal flux reference tables computed according to speed and load torque values. Section 3 presents the implementation of the optimization technique for the scalar control structure of the IM. Simulation results are shown in section 4 and compared to experimental ones to validate the predicted efficiency improvement and the feasibility of the optimized control. Results are shown for two squirrel-cage induction motors, one complying with the IE2 standard, and the second with IE3 standards. Finally, conclusions are drawn.

2. Optimal Flux Tracking

2.1. Improved Dynamic Model

The representation of the squirrel-cage induction motor for analysis purposes is done through the classic dynamic model. It is used to predict the IM performance at transient and steady state of operation, and is based on electrical, flux and mechanical equations, where the following parameters need to be known:

R_s	resistance of a stator phase winding
R_r	squirrel-cage rotor resistance
L_s	self-inductance of a stator phase winding
L_r	squirrel-cage rotor self-inductance
M_{sr}	stator-rotor mutual inductance
σ	motor dispersion coefficient $\left(\sigma = 1 - \frac{M_{sr}^2}{L_s L_r}\right)$
p	number of pole pairs of the motor
J	total motor and load inertia
f_v	viscous friction coefficient
T_0	dry friction torque

The electrical equations of the model can be schematically represented in the stationary reference frame as in Fig. 1.

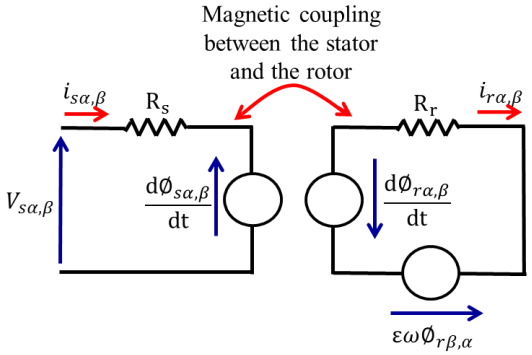

Fig. 1. α, β-axis IM classic representation. $\varepsilon = 1$ for the α-axis and -1 for the β-axis.

In this representation, the only losses that appear are the copper losses, represented by the stator and rotor resistors. In addition, friction losses are taken into account through the mechanical equation of the IM. Core losses are therefore not taken into consideration through this model, and shall be introduced in order to insure the most accurate representation possible.

The core losses can be introduced in the dynamic model electrical equations of the IM through an equivalent resistor. The latter can be computed through a no-load test on the motor at rated speed. However, the obtained value would not be accurate enough to estimate the losses in transient state operation, or in cases of speed and voltage values different from the rated ones.

Indeed, these losses are the result of hysteresis effect, Eddy currents and imperfections in the magnetic circuit. They are affected by the voltage signal frequency and the magnetic field amplitude as detailed in [7]. Consequently, they can be estimated by the model shown in (1).

$$P_c(t) = K_H B_{max}^2(t) f(t) + K_E f^2(t) \sum_k k^2 B_k^2(t) + K_{ex} f^{1.5}(t) \sum_k k^{1.5} B_k^{1.5}(t) \quad (1)$$

B_{max} and B_k represent respectively the maximal amplitude and the k^{th} harmonic amplitude of the magnetic field, f the voltage frequency, and K_H, K_E and K_{ex} respectively the coefficients of the hysteresis effect, the Eddy Currents effect, and the excess core losses.

The core losses equivalent resistor can then be computed continuously using the losses model, as shown in (2).

$$R_c(t) = \frac{1}{P_c(t)}\left[\left(V_{s\alpha}(t) - \mathrm{R_s} i_{s\alpha}(t)\right)^2 + \left(V_{s\beta}(t) - \mathrm{R_s} i_{s\beta}(t)\right)^2\right] \quad (2)$$

V_{sx} represent the stator voltages and i_{sx} the stator currents in the stationary reference frame, with $x = \alpha, \beta$.

The computed equivalent resistor can be included, as detailed in [8], in the stationary reference frame dynamic model of the IM as represented in Fig. 2, based on the classic IM steady-state model which takes core losses into consideration.

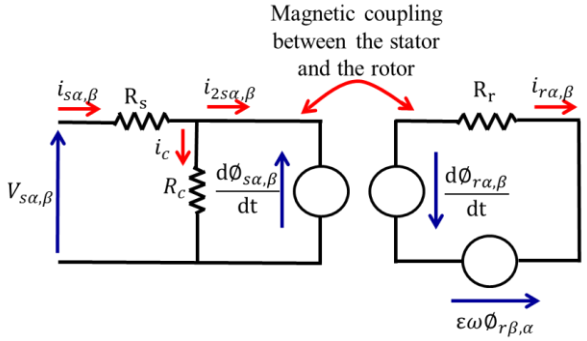

Fig. 2. α, β-axis IM representation with core losses resistor. $\varepsilon = 1$ for the α-axis and -1 for the β-axis.

Accordingly, the currents used in the flux equations of the IM are changed from $i_{s\alpha}$ and $i_{s\beta}$ in the classic dynamic model, to $i_{2s\alpha}$ and $i_{2s\beta}$ in the improved model taking core losses into account, as shown in (3).

$$\begin{cases} i_{2s\alpha}(t) = i_{s\alpha}(t) - \dfrac{1}{R_c(t)}\dfrac{\mathrm{d}\emptyset_{s\alpha}(t)}{\mathrm{dt}} \\ i_{2s\beta}(t) = i_{s\beta}(t) - \dfrac{1}{R_c(t)}\dfrac{\mathrm{d}\emptyset_{s\beta}(t)}{\mathrm{dt}} \end{cases} \quad (3)$$

Consequently, the flux equations are changed while the electrical equations are the same as the classic IM dynamic model. By applying the Park transform to the improved IM dynamic model, the obtained flux and electrical equations in the rotating reference frame, are represented in (4) to (11).

- Flux equations

$$\emptyset_{sd} = \mathrm{L_s} i_{sd} - \frac{\mathrm{L_s}}{R_c}\left[\frac{d\emptyset_{sd}}{dt} - \omega_d \emptyset_{sq}\right] + \mathrm{M_{sr}} i_{rd} \quad (4)$$

$$\emptyset_{sq} = \mathrm{L_s} i_{sq} - \frac{\mathrm{L_s}}{R_c}\left[\frac{d\emptyset_{sq}}{dt} + \omega_d \emptyset_{sd}\right] + \mathrm{M_{sr}} i_{rq} \quad (5)$$

$$\emptyset_{rd} = \mathrm{L_r} i_{rd} + \mathrm{M_{sr}} i_{sd} - \frac{\mathrm{M_{sr}}}{R_c}\left[\frac{\mathrm{d}\emptyset_{sd}}{\mathrm{dt}} - \omega_d \emptyset_{sq}\right] \quad (6)$$

$$\emptyset_{rq} = \mathrm{L_r} i_{rq} + \mathrm{M_{sr}} i_{sq} - \frac{\mathrm{M_{sr}}}{R_c}\left[\frac{\mathrm{d}\emptyset_{sq}}{\mathrm{dt}} + \omega_d \emptyset_{sd}\right] \quad (7)$$

- Electrical equations

$$V_{sd} = \mathrm{R_s} i_{sd} + \frac{\mathrm{d}\emptyset_{sd}}{\mathrm{dt}} - \omega_d \emptyset_{sq} \quad (8)$$

$$V_{sq} = \mathrm{R_s} i_{sq} + \frac{\mathrm{d}\emptyset_{sq}}{\mathrm{dt}} + \omega_d \emptyset_{sd} \quad (9)$$

$$0 = \mathrm{R_r} i_{rd} + \frac{\mathrm{d}\emptyset_{rd}}{\mathrm{dt}} - (\omega_d - \omega)\emptyset_{rq} \quad (10)$$

$$0 = \mathrm{R_r} i_{rq} + \frac{\mathrm{d}\emptyset_{rq}}{\mathrm{dt}} + (\omega_d - \omega)\emptyset_{rd} \quad (11)$$

Where $\emptyset$, i and V represent respectively the flux, current and voltage variables, ω the electrical speed of the rotor, and ω_d the angular speed of the rotating frame. Subscripts s and r refer to the stator and rotor of the IM, and d and q to the rotating reference frame axes.

The improved dynamic model is simulated and experimentally validated in [8], and thus proven to give an accurate representation of the IM performance and core losses variations according to the operating point.

2.2. Best Efficiency Point

In order to increase the energy efficiency of the motor, by tracking the best efficiency point, calculations are made to estimate its values according to the operating conditions, in terms of load torque, speed and stator flux. Therefore, the estimation is done according to (12).

$$\eta = \frac{T_{em}.\Omega - P_{mec}}{P_{in}} \quad (12)$$

Where,

T_{em}	electromagnetic torque: $T_{em} = \mathrm{p.M_{sr}}.Im(\bar{\imath_s}.\bar{\imath_r}^*)$
P_{mec}	mechanical losses: $P_{mec} = \mathrm{f_v}\Omega^2 + \mathrm{T_0}\Omega$
P_{in}	input power: $P_{in} = Re(\bar{V_s}.\bar{\imath_s}^*)$
Ω	mechanical speed of the rotor
$\bar{V_s}$	stator voltage phasor: $\bar{V_s} = V_{sd} + jV_{sq}$
$\bar{\imath_s}$	stator current phasor: $\bar{\imath_s} = i_{sd} + ji_{sq}$
$\bar{\imath_r}$	rotor current phasor: $\bar{\imath_r} = i_{rd} + ji_{rq}$

By replacing the improved dynamic model equation (4) to (11) in (12), it is possible to compute the efficiency variations versus the stator flux, the speed and the angular speed of the rotating frame ω_d. The latter is computed according to the load torque $\mathrm{T_L}$ through the mechanical equation of the IM written at steady state as in (13).

$$T_{em} = f_v \Omega + T_0 + T_L \quad (13)$$

Therefore, calculations are carried to plot the variation of the energy efficiency according to the operating conditions. Results show that the best efficiency zone corresponds to an optimal flux value that varies according to the load torque and the speed. For example, for a 5.5kW induction motor, at rated speed, while operating at load torques less than 56% of rated torque, the best efficiency point is reached for stator flux values that are below the rated flux.

Results are shown in Fig. 3 for a simulation at a load of 14% rated torque. The contours represent the efficiency values, and are scaled in 'per unit' values of the rated motor characteristics. The best efficiency zone is obtained for values of 40 to 70% of rated stator flux, depending on the operating speed. The computed values of energy efficiency are experimentally validated in [8] for various loads.

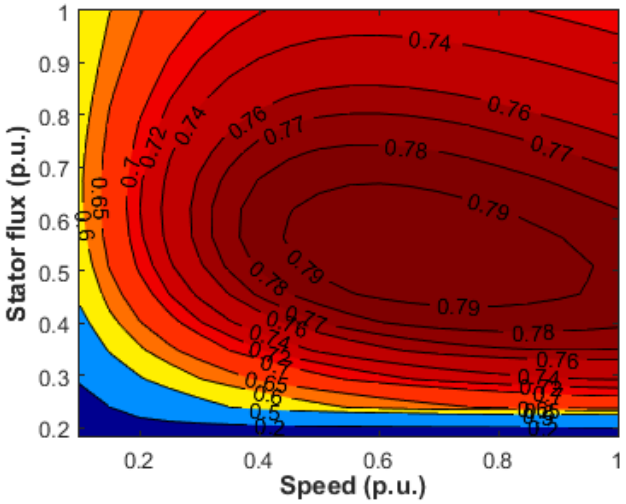

Fig. 3. Energy efficiency variation at 14% rated torque.

2.3. Optimal Flux

The operating conditions, in terms of load torque and rotation speed, of an induction motor are imposed by the user according to the driven load. Therefore, the best efficiency point can be tracked by modifying the stator flux through the control system.

In order to avoid on-line calculations while operating an induction motor, the optimal stator flux values are computed through similar calculation as in 2.2 and stored in a look-up table. These calculations are done for every possible operating point corresponding to the best energy efficiency.

Fig. 4 shows the results of the optimal stator flux, in 'per unit' of the rated flux, versus to the operating torque and speed. The optimal values of flux obtained are based on the IM dynamic model including core losses, which improve? the accuracy of the estimated optimal operating point.

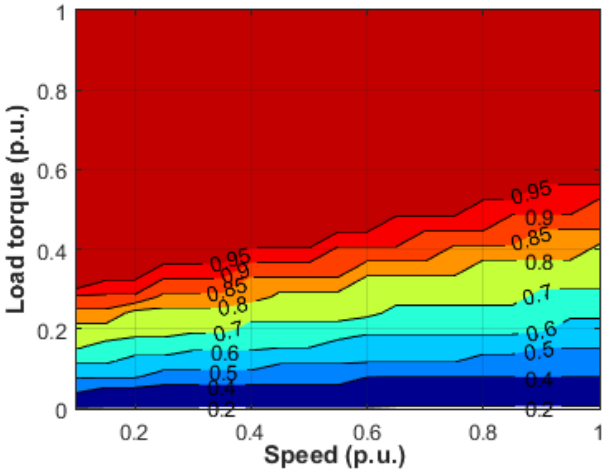

Fig. 4. Optimal flux (p.u.).

3. Scalar Control Optimization

3.1. Conventional Scalar Control

Scalar control is one of the well-known controls used in the case of induction motors, in several applications because of its simple structure and ease of implementation. The stator voltage reference amplitude is computed for a given flux reference and frequency value [9], through a scalar control law as shown in (14).

$$V_s = \frac{L_s \emptyset_s}{R_s} \sqrt{\frac{\left(\frac{L_s \omega_s}{R_s} + \frac{L_r \omega_r}{R_r}\right)^2 + \left(1 - \frac{\sigma L_s L_r \omega_s \omega_r}{R_s R_r}\right)^2}{1 + \left(\frac{\sigma L_r \omega_r}{R_r}\right)^2}} \quad (14)$$

Furthermore, a speed regulator is included in order to reach the speed reference value at steady-state and to compensate the slip effect. This stator voltage angular frequency ω_s is obtained by the autopilot technique as the sum of the rotor angular frequency ω_r and the actual electrical speed ω of the IM.

3.2. Optimized Control Structure

The conventional scalar control guarantees the operation of the induction motor at the required flux and speed according to the given references. Therefore, it is possible to impose the stator flux, in order to reach the desired optimized flux detailed in 2.3.

According to the look-up table shown in Fig. 4 the optimal flux tracking requires the knowledge of the actual speed of the motor and the load torque values. Therefore, the scalar control flux reference is updated as in Fig. 5.

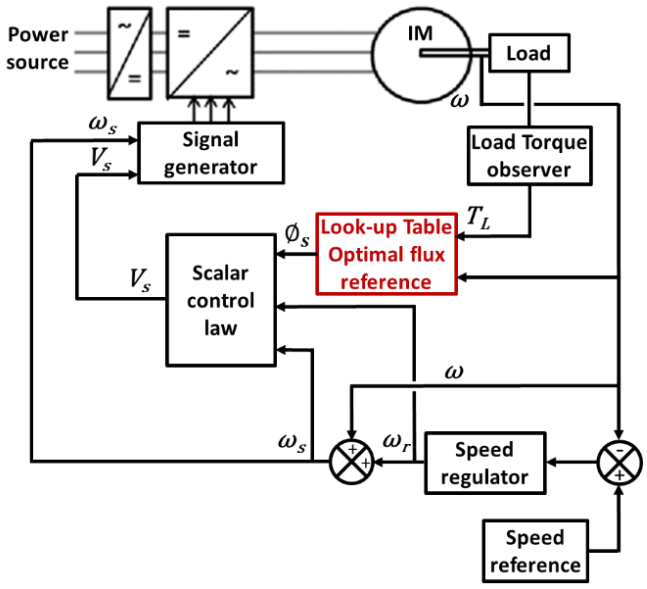

Fig. 5. Optimized scalar control

The load torque value necessary for the choice of the stator flux is estimated by a first order Luenberger torque observer [10]. For this purpose, the mechanical equation of the IM is used and the load torque is considered to be constant on every sampling period, as in (15).

$$\begin{cases} \frac{d\Omega}{dt} - \frac{T_{em}}{J} + \frac{f_v}{J}\Omega + \frac{T_0}{J} + \frac{T_L}{J} = 0 \\ \frac{dT_L}{dt} = 0 \end{cases} \quad (15)$$

The equations in (15) are written in a state-space representation and a first order Luenberger observer is included through the Luenburger factor l to minimize the estimation error of the torque load. Equation (16) is obtained, where $\widehat{T_L}$ is the observed torque load, and T_L is the estimated torque load form the mechanical equation using the measured speed of the IM.

$$\frac{d\widehat{T_L}}{dt} = \left(\frac{1}{J} - l\right)\widehat{T_L} - \frac{T_{em}}{J} + \frac{f_v}{J}\Omega + \frac{T_0}{J} + \frac{d\Omega}{dt} + lT_L \quad (16)$$

The electromagnetic torque is estimated via the classic equation shown in (17).

$$T_{em} = p\frac{M_{sr}}{\sigma L_s L_r}\left(\emptyset_{r\alpha}\emptyset_{s\beta} - \emptyset_{s\alpha}\emptyset_{r\beta}\right) \quad (17)$$

The stator flux values necessary for computing the electromagnetic torque are estimated using the IM dynamic model electrical equations in the stationary reference frame as in (18).

$$\emptyset_{s\alpha\beta} = \int \left(V_{s\alpha\beta} - R_s i_{s\alpha\beta}\right)dt \quad (18)$$

The proposed control structure in Fig. 5 allows the modification of the stator flux reference in the control system according to the operating point, in order to reach the optimized energy efficiency in the IM, while taking into account the copper, core and mechanical losses.

4. Experimental Results

4.1. Experimental Test Bench

The proposed optimized control scheme is tested experimentally on a Leroy-Somer 5.5kW squirrel-cage induction motor, compliant with IE2 energy efficiency standard. The test bench, shown in Fig. 6, consists of the IM fed by a Semikron inverter, controlled by a dSpace driver. The reference voltages are computed through the optimized scalar control system. The DC bus is loaded and regulated through an autotransformer and a rectifier. The IM drives a direct current motor which constitutes the torque load, and suitable voltage, current and speed sensors are used for the controller feedback and the torque observer.

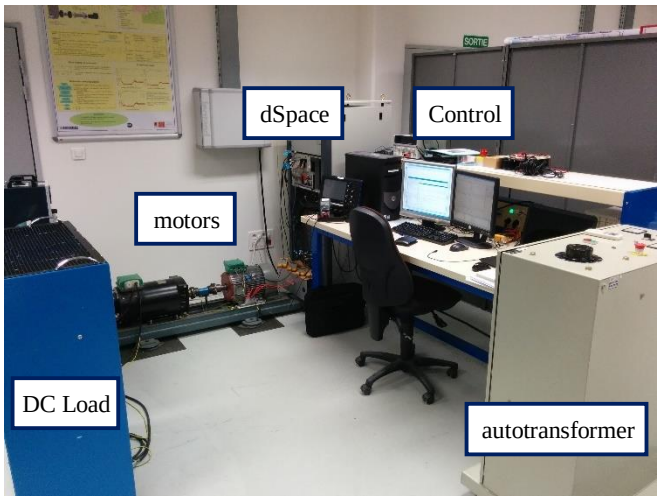

Fig. 6. Test bench

The control system is implemented in Matlab/Simulink to simulate the IM performances with the improved scalar control, and to implement the actual control in the dSpace driver. The main losses of the system, as well as the input power and the energy efficiency are computed through the tests.

4.2. Operating Conditions

A series of experiments on the studied motor allows the computation of its parameters and core losses model coefficients. The parameters are used to simulate the motor as defined in 2.1, and to run the scalar control function (14). On the other hand, the core losses coefficients are computed to evaluate the core losses in both tests and simulations, the most accurately possible according to (1).

Simulations and tests are done for a series of operating points, but the presented results correspond to an operation at 50% of rated speed and 25% of rated torque. The

optimization technique modifies the stator flux reference to match the best efficiency point. However, at low speed and load, the given flux reference in the look-up table of Fig. 4 is less than 10% of the rated value. Therefore, at start-up phase, the rated flux is established first in order to ensure a proper start-up of the motor, then the control optimization is launched to set the optimal stator flux and improve the efficiency.

In the experimental and simulation results shown, the steady-state is already established at time t=0s for 50% of rated speed and 25% of rated torque of the studied motor. Then at t=3s, the optimization procedure is applied to show the difference with the classical scalar control performances.

The operating conditions of the tests and simulations are represented in the following graphs: the stator flux reference in Fig. 7, the reference and actual speed of the motor in Fig. 8, and the load and electromagnetic torques in Fig. 9.

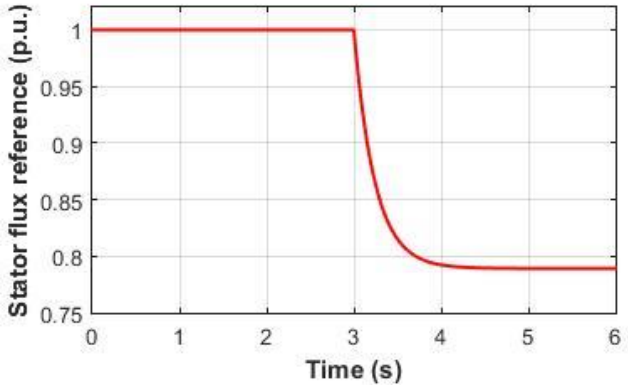

Fig. 7. Simulated stator flux reference.

The optimization process is shown in Fig. 7 which shows that the stator flux reference decreases at t=3s to meet the optimized value defined in the look-up table according to the speed and load torque.

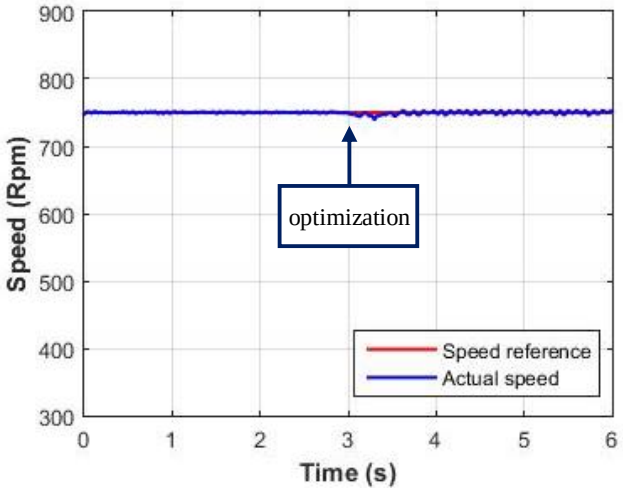

Fig. 8. Simulated speed.

A slight distortion in the speed curve takes place when the stator flux is instantly modified, then the steady-state is established again as it can be seen in Fig. 8.

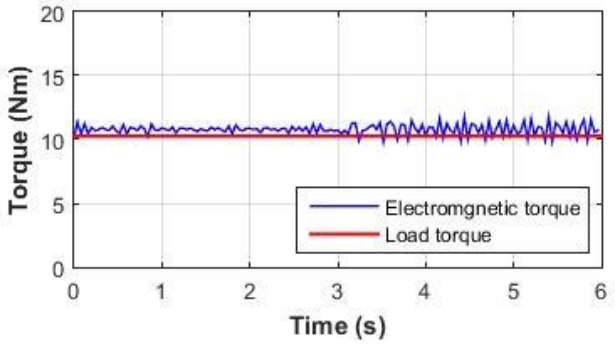

Fig. 9. Simulated electromagnetic and load torque.

Fig. 9 shows that the electromagnetic torque is also affected by the stator flux variation which causes a transient phase before reaching the same previous steady-state in the end.

4.3. Experimental Energy Results

The variations of flux, speed and torque show the temporary effect of the optimization technique on the steady state phase that is immediately reinstated, in the dynamics of the motor. On the other hand, the effect of this technique appears clearly in the energy analysis of the motor, in terms of losses as shown in Fig. 10 and Fig. 11, of input power as in Fig. 12, and energy efficiency in Fig. 13, which is indeed the main scope of the optimization.

The flux reduction causes the reduction of voltages and currents in the motor, in order to reduce the excess of lost power in the motor while running at rated flux and low torque. As a result, the copper losses and the core losses are reduced when the optimization is applied as presented in Fig. 10 and Fig. 11. The simulation results are validated experimentally as shown in the graphs with average relative errors of 1.76% for the copper losses and 1.27% for the core losses.

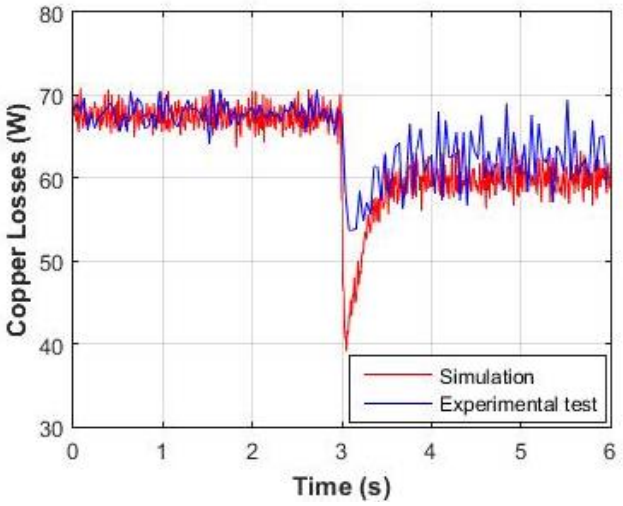

Fig. 10. Simulated and experimental copper losses.

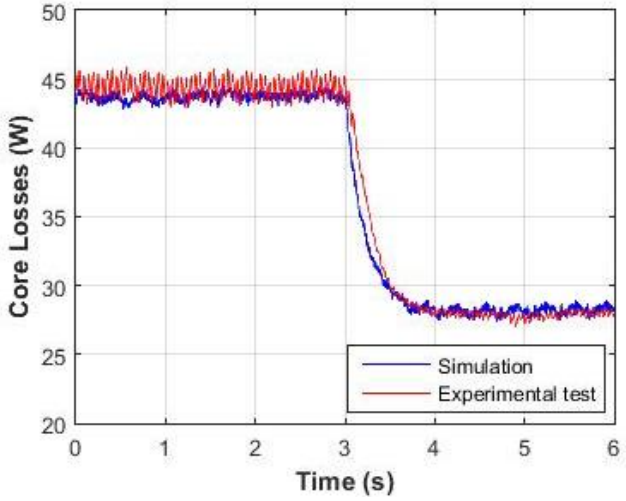

Fig. 11. Simulated and experimental core losses.

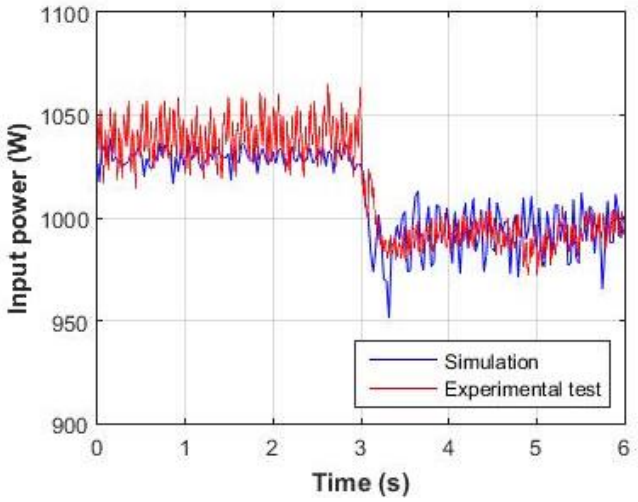

Fig. 12. Simulated and experimental input power.

The input power, like ? the power losses is reduced through the optimization and the experimental results validate the simulation with 0.73% average error.

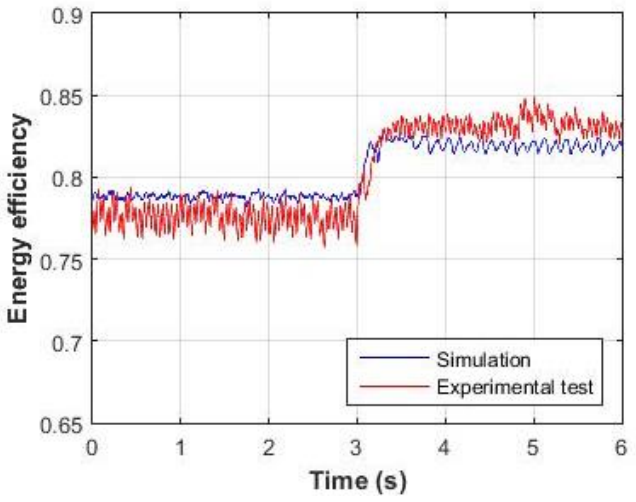

Fig. 13. Simulated and experimental energy efficiency.

The essential part of the optimization lies in the energy efficiency of the motor which is proven to increase by 5.5% as predicted through the simulation, with a satisfactory error of 1.36%. It is important to note that the increase in efficiency is higher at lower values of load torque, and can reach 15 to 20% of increase while operating at around 14% of rated torque.

Further to the presented improvement in the losses and power inside the induction motor, a simulation of the losses inside the inverter is done and shown in Fig. 14. These calculations of the conduction and commutation losses of the inverter are based on the switches characteristics provided by the constructor. These losses decrease through the optimization process due to the currents reduction. This result confirms that the improvement affects the entire inverter-motor system efficiencyand not only the IM.

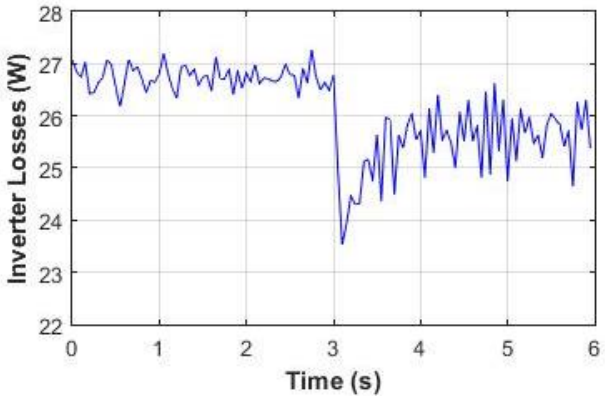

Fig. 14. Simulated inverter losses.

4.4. Experimental Validation

The presented results correspond to a single operating point of 50% speed and 25% load torque. However, according to standard IEC 60034-30-2 used by manufacturers like Leroy-Somer, the motor performances are validated experimentally at a range of operating points of speed and load which are represented in the graph of Fig. 15.

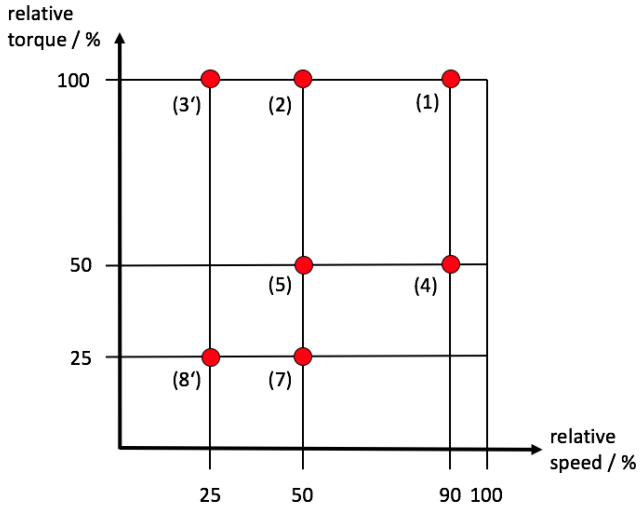

Fig. 15. Experimental validation operating points.

Tests of the optimized scalar control have been made on most of these points except the 100% torque points which could not be reached because of the available DC motor power which could ensure in the best cases 65% of rated torque at 90% speed. The obtained experimental efficiency results were compared to the theoretical ones and the errors shown in table I where T_n represents the rated torque and Ω_s the synchronous speed.

I. Experimental vs simulated efficiency error

	25% T_n	**50% T_n**	**65% T_n**
25% Ω_s	1.28%	-	-
50% Ω_s	1.36%	0.51%	0.65%
90% Ω_s	0.24%	0.11%	0.11%

The results show satisfactory ranges of errors which are mainly caused by the measuring instruments ? and the effect of harmonics and signal filtering aiming to obtain the most accurate values possible. Therefore, the optimization study and the simulated performances of the motor are validated experimentally.

4.5. IE3 Motor Experimental Validation

Further to the tested case and as mentioned in section 1, premium efficiency motors are manufactured to comply with the new IE3 standard of construction. These motors have a higher range of efficiencies compared to the IE2 motors. Therefore, in order to verify the compatibility of the proposed optimization technique with more recent motors, tests have been done on another 5.5kW Leroy Somer motor compliant with IE3 energy efficiency standard.

The differences between the experimental and theoretical efficiency results at the operating points defined by the standards are presented in table II. The results are also satisfactory.

II. Experimental vs simulated efficiency error – IE3 motor

	25% T_n	**50% T_n**	**65% T_n**
25% Ω_s	0.51%	-	-
50% Ω_s	1.91%	2.34%	0.12%
90% Ω_s	0.12%	1.58%	0.67%

5. Conclusion

An optimization technique of the scalar control scheme of squirrel-cage induction motors has been presented in the paper, showing its effect on the power losses and on the efficiency especially at low load and speed operating conditions.

The proposed structure is based on an improved dynamic model of the IM which takes core losses into account. A look-up table is built containing the optimal stator flux values corresponding to the best energy efficiency for the entire range of possible operating points. The output of this table is used as the stator flux reference of the scalar control scheme. Simulations and tests are conducted on two 5.5kW motors, one compliant with IE2 standard, and the other with IE3 standard, in order to validate the efficiency improvement of both motors with the proposed optimization, as well as a decrease in the inverter losses.

Based on the evaluation of the main losses in the motor, other structures of optimization can be developed using different approaches or online calculations and applied to other types of control as the vector or torque control of the induction motors. In a future study, the proposed optimization technique shall be tested on the field-oriented vector control scheme to prove its compatibility with other types of control.

6. Appendix: Motors Characteristics

The characteristics of the IE2 Leroy-Somer 5.5kW squirrel-cage induction motor used in the experiments are listed in table III.

III. IE2 Leroy-Somer 5.5kW IM characteristics

U_n	400 V	**R_s**	0.86 **Ω**
I_n	11.9 A	R_r	0.83 **Ω**
Ω_n	1455 Rpm	L_s	163 mH
p	2	L_r	163 mH
J	0.0157 kg. m^2	M_{sr}	157 mH
f_v	0.003137 kg. m^2. s^{-1}	T_0	0.2573 N.m

The characteristics of the IE3 Leroy-Somer 5.5kW IM used in the second series of experiments are listed in table IV.

IV. IE3 Leroy-Somer 5.5kW IM characteristics

U_n	400 V	**R_s**	0.87 **Ω**

I_n	10.4 A	R_r	0.7 **Ω**
Ω_n	1462 Rpm	L_s	163 mH
p	2	L_r	163 mH
J	0.02286 $kg.m^2$	M_{sr}	158 mH
f_v	0.003295 $kg.m^2.s^{-1}$	T_0	0.2711 N.m

The characteristics of the 3.9kW Leroy Somer DC motor used to create the load torque are listed in table V.

V. DC Leroy-Somer 3.9kW characteristics

$\mathbf{U_n}$	260 V	$\mathbf{\Omega_n}$	1450 Rpm
$\mathbf{I_n}$	17.6 A	**J**	0.05 $\mathbf{kg.m^2}$

ACKNOWLEDGEMENTS

The authors acknowledge the support of the Research Council and the CINET research center of the Université Saint-Joseph de Beyrouth (USJ), the Agence Universitaire de la Francophonie AUF, the Lebanese National Council for Scientific Research CNRS and the LAPLACE research center.

REFERENCES

[1] C. Thanga Raj, S. Srivastava, and P. Agarwal, *Energy Efficient Control of Three-Phase Induction Motor - A Review*, International Journal of Computer and Electrical Engineering, Vol. 1, No. 1, April 2009.

[2] J. Cleland, V. McCormick, and M. Turner, *Design of an Efficiency Optimization Controller for Inverter-fed AC Induction Motors*, Industry Applications Conference, Florida, 1995.

[3] M. Waheedabeevi, A. Sukeshkumar, and N. Nair, *New online loss- minimization-based control of scalar and vector-controlled induction motor drives*, IEEE International Conference on Power Electronics, Drives and Energy Systems, India, 2012.

[4] Y. Li and H. Yu, *Energy-Optimized Fuzzy Control of Induction Motors Based on Nonintrusive Efficiency Estimation*, 16th IEEE International Conference on Control Applications, Singapore, October 2007.

[5] M. Cacciato, A. Consoli, G. Scarcella, G. Scelba, and A. Testa, *Efficiency Optimization Techniques via Constant Optimal Slip Control of Induction Motor Drives*, International Symposium on Power Electronics, Electrical Drives, Automation and Motion, Italy, 2006.

[6] N. Sidek, N. Rosmin, H. Rahman, M. Hassan, F. Hussin and A. Musta'amal, *Efficiency Optimization of an Induction Machine using Optimal Flux Control*, IEEE Conference on Energy Conversion, Malaysia, 2014.

[7] F. Fiorillo, A. Novikov, *An Improved Approach to Power Losses in Magnetic Laminations under Nonsinusoidal Induction Waveform*, IEEE Transactions On Magnetics, vol. 26, no. 5, pp. 2904 – 2910, September 1990.

[8] G. Khoury, R. Ghosn, F. Khatounian, M. Fadel, M. Tientcheu, *An improved Dynamic Model for Induction Motors Including Core Losses*, IEEE International Conference on Power Electronics and Motion Control, Bulgaria, 2016.

[9] S. Nasar, I. Boldea, *Electric Machines Dynamics and Control*, CRC Press, pp.113-184, 1993.

[10] S. El Khil, I. Slama-Belkhodja, M. Pietrzak-David, B. de Fornel, *Sensorless Field Oriented Control of Doubly Fed Induction Speed Drive*, The International Conference on "Computer as a Tool", Warsaw, September 2007.